(This article is a preprint of the final article that appeared in the 1994 IEEE Ultrasonics Symposium Proceedings, pp. 1027-1032)

TIME-DOMAIN MODELING OF COMPOSITE ARRAYS FOR UNDERWATER IMAGING

G. L. Wojcik, D. K. Vaughan, V. Murray†, and J. Mould, Jr.
Weidlinger Associates, 4410 El Camino Real, Suite 110, Los Altos, CA 94022, U.S.A.
†UDI-Wimpol Limited, Denmore Road, Bridge of Don, Aberdeen AB23 8JW, Scotland

ABSTRACT

Time-domain, finite element simulations are used to explore some design issues and the practical modeling envelope for 1-3 composite arrays in underwater pulse-echo imaging transducers. This provides a relatively new perspective on the design problem via large-scale 2D and 3D transient simulations that include many piezoelectric pillars within the composite. Cross-talk from a prototype 150 kHz array is modeled and compared to data. Some of the composite slab's dispersion behavior is derived from its impulse response and used to interpret cross-talk. Numerical experiments on a 500 kHz design demonstrate effects of pillar taper and distribution—freedoms offered by injection molding. Fourier optics manipulation of the projected acoustic field is illustrated. These studies support an ongoing design and fabrication collaboration under the aegis of United States and Commonwealth naval agencies. Our role is to provide multi-dimensional, global modeling methods that complement semi-analytical approaches, as part of an effort to increase performance of broadband imaging sonars in the 100 kHz to 1 MHz range.

INTRODUCTION

Composite transducers are *engineered piezoelectric multiphase materials* tailored to the design tradeoffs in acoustic array applications [1,2]. Our interest is in modeling composites with 1-3 connectivity, namely, 1D-connected piezoceramic (pillars or rods) in 3D-connected polymer (matrix). A typical layout is illustrated in Fig. 1 from a 150 kHz prototype. This $\lambda/2$ thickness-resonant block is sandwiched between a backing material and impedance matching layer(s) for pulse-echo imaging applications. 1-3 composites are conventionally manufactured by the dice-and-fill technique, which is rather labor intensive but nonetheless quite effective. An injection molding method for the piezoceramic [3] has recently bee developed to the point that it offers significant advantage certainly in cost for high volume applications, and likely performance as well. A good overview of fabrication tec nologies and tradeoffs is given in [4].

The principal electromechanical advantages of 1-3 piezoceramic composites, over single phase transducer materials, are higher coupling in the thickness mode, lower mechanical impedance, reduced lateral mode interference, and better electrical load matching. Low lateral cross-talk and broadband behavior are achievable by choices of composite phases and layout, e.g., piezoceramic volume fraction, pillar shape, alignment and spacing, electrode coverage, as well as matching layer(s) and backing. Unfortunately, design tradeoffs are generally exclusive, e.g., bandwidth versus transmitted power.

Composite designs are usually based on 1D [5], equivalent medium [6], and Bragg scattering [7,8] analyses. They are further refined via prototype experiments. In many cases this is sufficient, but poorly quantified 2D and 3D wave phenomena can still degrade performance. To better understand and accommodate these multi-dimensional effects, researchers and designers are trying to rely on numerical modeling, e.g., [9]. For various reasons this has been restricted to implicit, frequency-domain analysis in relatively small-scale models, e.g., a few composite cells with lateral periodicity in geometry and excitation. However, by applying a time-domain finite element algorithm to the electromechanical equations we are able to increase the scale and scope of feasible simulations substantially [10].

Time-domain, finite element modeling is a design and experimentation tool. It complements traditional theory and experiment by combining them in a computer setting with the potential for much *higher resolution* of electromechanical phenomena. In principal it is only limited by knowledge of the model's geometry, material properties, and boundary (interface) conditions. In practice, of course, modeling is also limited by computer resources. These are less of an issue now, with the ascendance of UNIX workstations, powerful PCs, and inexpensive memory. The need for complete model characterization is the principal modeling limitation today. How-

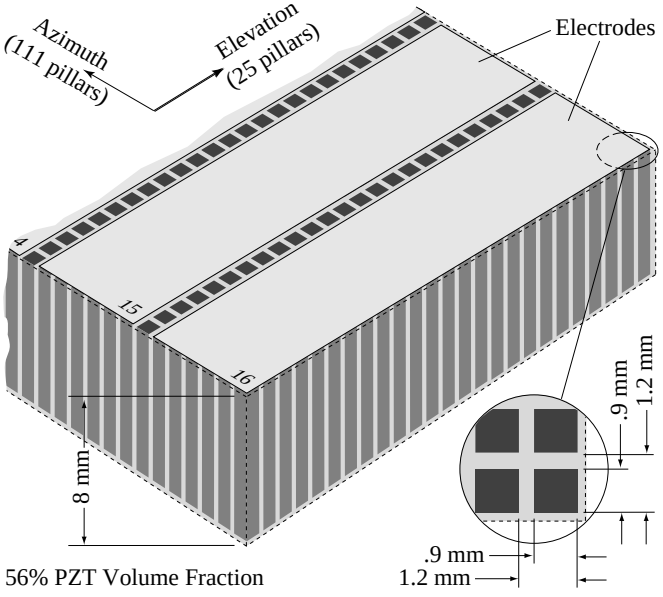

Figure 1. Drawing of pillar and electrode details in a 150 kHz 1-3 composite block. This is a prototype for an electronically scanned imaging sonar manufacured by UDI-Wimpol, Ltd.

ever, this need should not be looked upon as a bane. Even in the context of traditional methods it is incumbent upon designers to know their materials, otherwise faulty interpretations are inescapable.

The modeling applied here to 1-3 composites is intended to support a design and fabrication effort that includes United States and Commonwealth naval agencies, contractors, and universities. One of the principal objectives is to build and demonstrate broadband, high resolution imaging arrays for target characterization using injection molded 1-3 composites built by Material Systems, Inc. [3]. What follows is a preliminary exploration of modeling requirements and techniques for an evolving collaboration between ourselves, Prof. Gordon Hayward's Ultrasonics Research Group at the University of Strathclyde, Glasgow, Scotland, and Charles Desilets at Ultrasound Solutions, Inc.

TIME-DOMAIN MODELING

Under a National Science Foundation SBIR grant [11] we recently added piezoelectric and acoustic capabilities to our production finite element wave propagation code. This core code has been used by us and others over the last 13 years for large-scale, 2D/3D modeling in applications ranging from seismology and geophysics to nonlinear shock and vibration of structures to integrated optics and IC microlithography. The difference between our approach to transducer analysis and virtually every other discrete method reported is that we solve the spatially discretized electromechanical equations in the time-domain using a mixed explicit/implicit algorithm. The prevailing implicit finite element algorithm for transducer problems was first described in [12] and similar approaches have been applied regularly since, e.g., [13-18], with ANSYS [19], filling the commercial niche lately.

Explicit time integration is well known and arguably the most natural method for calculating broadband, wave-type phenomena. It is used primarily in the context of finite difference spatial discretizations (rather than finite element) and the underlying theory was well documented over 66 years ago [20]. In fact, it provided the basis for some of the first numerical solutions of partial differential equations on a digital computer [21]. Our explicit time-domain code, PZFlex, which incorporates facets of both finite difference and finite element discretizations, is described in [10] with validations and illustrative applications. During the last 18 months it has been used within the U.S. medical ultrasound industry and achieved wide acceptance.

PZFlex combines explicit solution of the dynamic elastic and acoustic fields with implicit solution of the quasi-static electric field, i.e., it applies an optimal solver to each electromechanical equation. The implicit electric field calculation is done directly (Gaussian elimination) or iteratively (preconditioned conjugate gradient), depending on problem size and dimension. Both the explicit integrator and the iterative solver operate on an element by element basis. The importance consequence is that computer resource requirements grow linearly with the number of elements, rather than as some power, which is the case for fully implicit, direct methods. Thus, our approach eliminates manipulation of large, sparse, symmetric systems of equations. It can therefore solve much larger problems, generally 100x-1000x, or execute the same size problem much faster, typically >100x, and is more amenable to vectorization and parallelization.

Models are composed of rectangles in 2D and bricks in 3D. These finite elements may be skewed but we make every effort to keep them Cartesian, permitting much faster model definition and problem execution. Only in the exceptional situation is accuracy degradation a problem, in which case the grid is typically refined. Integration time step is chosen automatically by the code to be less than the shortest transit time of the fastest electromechanical wave between adjacent nodes in the model. Models are necessarily truncated in space, where a high efficiency radiation boundary is applied (in any medium) to suppress nonphysical reflections. The model's electromechanical properties are fully anisotropic and damping include mass-proportional, stiffness-proportional, Rayleigh, viscoelastic, and viscous, each of which has a characteristic frequency dependence. Specification of arbitrary frequency dependence in the time-domain remains an active topic of research, e.g., [22]. Circuitry in the form of RLC networks and transmission lines are incorporated directly in the time-domain solution algorithm. Pre- and post-processing, including PostScript graphics and on-screen movies, is an integral part of the code.

COMPOSITE ARRAYS

As a practical basis for modeling we use a 1-3 composite built by UDI-Wimpol, Ltd., Aberdeen, Scotland, for a pulse-echo imaging transducer in an electronically scanned 150 kHz prototype sonar system. The composite block is made of 0.9 x 0.9 x 9.4 mm PZT-5H pillars (Vernitron, see [7] for properties) separated by a 0.3 mm wide kerf filled with polymer (Araldite, $V_L \approx 2150\ m/s$, ρ=1120 kg/m^3). This gives a 1.2 mm pillar pitch and 56% PZT volume fraction. The complete block is 25 pillars (≈30 mm) in elevation and 111 pillars (≈133 mm) in azimuth. The top and bottom surfaces are electroded with every seventh row (in elevation) clear, defining a 16 element array with 8.5 mm electrode pitch and six pillar rows under each. Overall layout of the block is shown in Figure 1. The prototype transducer uses an 8.0 mm block between a 4.5 mm matching layer (Stycast, $V_L \approx 2800\ m/s$, ρ=1100 kg/m^3) and a backing block of filled polyurethane ($V_L \approx 2400\ m/s$, ρ=600 kg/m^3). Although various measurements have been made on the block and transducer, incomplete knowledge of wavespeeds, damping, and electroding discourages us from trying any but the simplest comparison pending further measurements.

In addition to the 150 kHz prototype we consider numerical experiments on a 500 kHz high resolution imaging

transducer design. PZT-5H pillars are 3.27 mm x .6 mm and the filler is epoxy (Ciba-Geigy CY1301/HY1300, $V_L \approx 2700$ m/s, $V_S \approx 1443$ m/s, $\rho = 1148$ kg/m^3). The matching layer is 1.23 mm thick (silicone rubber, $V_L \approx 1820$ m/s, $V_S \approx 549$ m/s, $\rho = 1050$ kg/m^3) and the backing is tungsten-filled epoxy (Ciba-Geigy CY208/HY956, $V_L \approx 716$ m/s, $V_S \approx 344$ m/s, $\rho = 6932$ kg/m^3). Layout, illustrated in Fig. 2, and materials were suggested in part by Desilets [23], and Hayward and Bennett [24]. At least three pillars are included across the electrode to increase electromechanical coupling [9]. At 500 kHz the wave length in water is λ_0 = 3 mm and the block's elevation dimension, d_e=6.6 mm, is chosen for a far-field (continuous wave) beam spread of $\angle_e = 27° \approx 2\sin^{-1}(\lambda_0 / 2d_e)$. Its azimuthal dimension, d_a=196 mm (8 joined 24 mm blocks, 64 electrodes total) is chosen so that beam spread $\angle_a \leq 1° \approx \lambda_0 / d_a$. We anticipate that this device will be manufactured by injection molding, which gives more latitude in pillar shape and distribution than the dice-and-fill approach. Consequently, this model is used to examine a few effects of pillar taper and distribution.

CROSS-TALK COMPARISON

Mechanical cross-talk is an intrinsic property of 1-3 composites given the 3D elastic connectivity. Cross-talk modeling is investigated by comparison to measurements on the 9.4 mm UDI block in air. This comparison minimizes model uncertainty since only PZT and one polymer are involved. Poisson ratio of 0.4 is assumed for the soft-set polymer and the shear modulus quality factor is assumed to be $Q_{shear} \approx 25$ at 150 kHz. Mechanical loadings by the electrodes and air are ignored. The 3D finite element model includes two neighboring electrodes on each side terminated by an absorbing boundary condition (with the last pitch replaced by average properties). All symmetries are used to reduce model size, namely, reflection in azimuth and thickness, and periodicity in elevation. The model is 25x300x8 = 60,000 elements and runs in 5.2 hours on an HP 715/75 workstation.

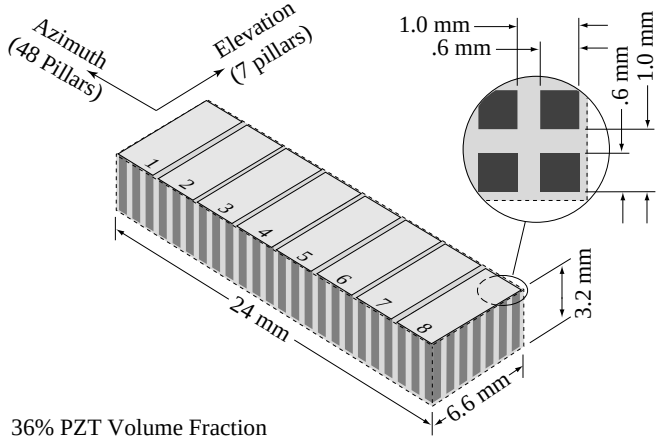

Figure 2. Drawing of pillar and electrode layout in a 500 kHz 1-3 composite design for high resolution imaging, to be made by injection molding. Eight blocks might be bonded end-to end to complete the array.

The measurement was made by driving an electrode near the center with a 3.6 μs, 10 V square wave and recording voltage at adjacent electrodes. Plots of data versus calculated cross-talk on the two neighboring electrodes are presented in Figure 3. The data show an initial pulse followed by a lower amplitude coda. Signal delays in the data give 1500 m/s for the initial pulse wavespeed. At the first electrode the calculation leads the first pulse slightly but agreement is generally good, while the coda is too high and out of phase. At the second electrode the calculation leads the first pulse significantly but still follows its form, while the calculated coda is much higher, about the same amplitude as at the closer electrode.

Electrical cross-talk to the adjacent electrode is apparent in the data during the 3.6 μs excitation but not in the simulation. Increasing dielectric constant in the polymer by a factor of 8 over the manufacturer's specified value (5 ε_0) yields a fit but this discrepancy is unreasonable. The 3D, time-dependent electric field calculation has been verified so we cannot explain the lack of electrical cross-talk from the model. In general, these results indicate that the code is able to simulate mechanical cross-talk in the composite block on a practical 3D scale.

DISPERSION ANALYSIS

Electromechanical waves propagating laterally in the composite are dispersed by its finite thickness and periodic structure. In other words, the characteristic lengths cause phase velocity

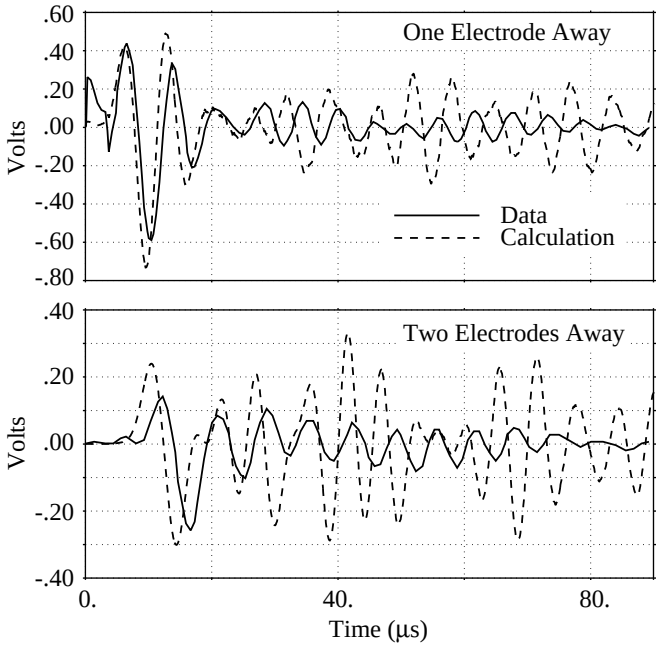

Figure 3. Comparison of measured and calculated cross-talk in the 9.4 mm UDI composite block at two electrodes next to the driven electrode.

to depend on frequency. Current theory [7,8] provides a qualitative understanding and guidelines for design, but is limited by the failure of classical analysis in realistic composites. In this regard numerical modeling is no panacea but it does permit some useful quantification of dispersion behavior in composite blocks.

To quantify dispersion, in azimuth say, the model must extend over many electrodes to allow sufficient time and distance to separate the wave phases. The computer memory required makes 3D models of the UDI block impractical. Therefore, a 2D cross-section through pillar centers is substituted—effectively representing the 1-3 by a 2-2 composite "plate," which ignores periodicity in elevation. Despite this approximation the predicted dispersion behavior should be close by virtue of incorporating the important characteristic lengths (block thickness and width and pitch of pillars and electrodes). Accuracy of the 2D model may be increased by using averaged properties in elevation while retaining detailed properties in azimuth, although this is not done here.

The method consists of impulsively driving the center electrode of the long 2-2 model and plotting normal velocity versus time at the top (center) of each pillar. This is a common means of presenting and analyzing seismic phases in geophysics, i.e., to identify body waves and surface waves or waveguide modes. The result is a plot of arrival time (vertical) versus distance (horizontal), shown in Fig. 4 for the block in air, where velocity (modified log) is plotted in gray-scale. Moving vertically above any pillar location shows the velocity time-history there and moving horizontally at any time shows the surface waveform along the model. Examples are plotted above the figure. By drawing a line through coherent arrivals we can identify discrete wave phases or groups. Slope of the line gives the wave slowness (inverse velocity, c), while vertical and horizontal spacing between peaks gives predominant period (inverse frequency, f) and wavelength, λ, related by $f=c/\lambda$.

Three coherent arrival loci are identified in Fig. 4 as S1, S2, and S3, ordered by increasing slowness (slope). S1 is the first arrival at any station, with a velocity (inverse slowness) of ≈1800 m/s, a predominant frequency of ≈120 kHz, and a wavelength of ≈15 mm. Since 1800 m/s is the average shear wave speed calculated in a 1D composite array model, S1 is a horizontally propagating shear (SV) wave in the 2D composite plate. No earlier phase is evident at higher magnification, hence, longitudinal precursors are virtually nonexistent. S2 yields a velocity of ≈1100 m/s, predominant frequency of ≈177 kHz, and wavelength of ≈6.2 mm. This is typically the highest amplitude signal in any record away from the driven electrode. S3 is the locus of S2 arrivals and indicates a velocity of ≈476 m/s. S2 and S3 correspond to a composite plate mode (Lamb-type wave) with phase velocity S2 and group velocity S3, i.e., signal and energy propagation speeds, respectively.

Figure 5 shows the same analysis for the in-situ block—inwater, sandwiched between matching and backing. Phase S0 appears as a precursor to S1 with velocity ≈ 2900 m/s, frequency ≈185 kHz, and wavelength ≈25.3 mm; it is the longitudinal wave through the matching layer. S2, the "SV" wave in the plate is slower now, ≈1600 m/s, ≈154 kHz, and ≈10.4 mm. Phase and group velocity of the plate wave, S2 and S3, are ≈1230 m/s and ≈540 m/s at a predominant frequency of ≈220 kHz and ≈5.6 mm wavelength. S2 velocity is close to the shear wave speed in the backing (1150 m/s). Another plate mode appears with phase velocity S4 ≈1320 m/s and group velocity S5 ≈320 m/s, at ≈220 kHz frequency and ≈6.0 mm

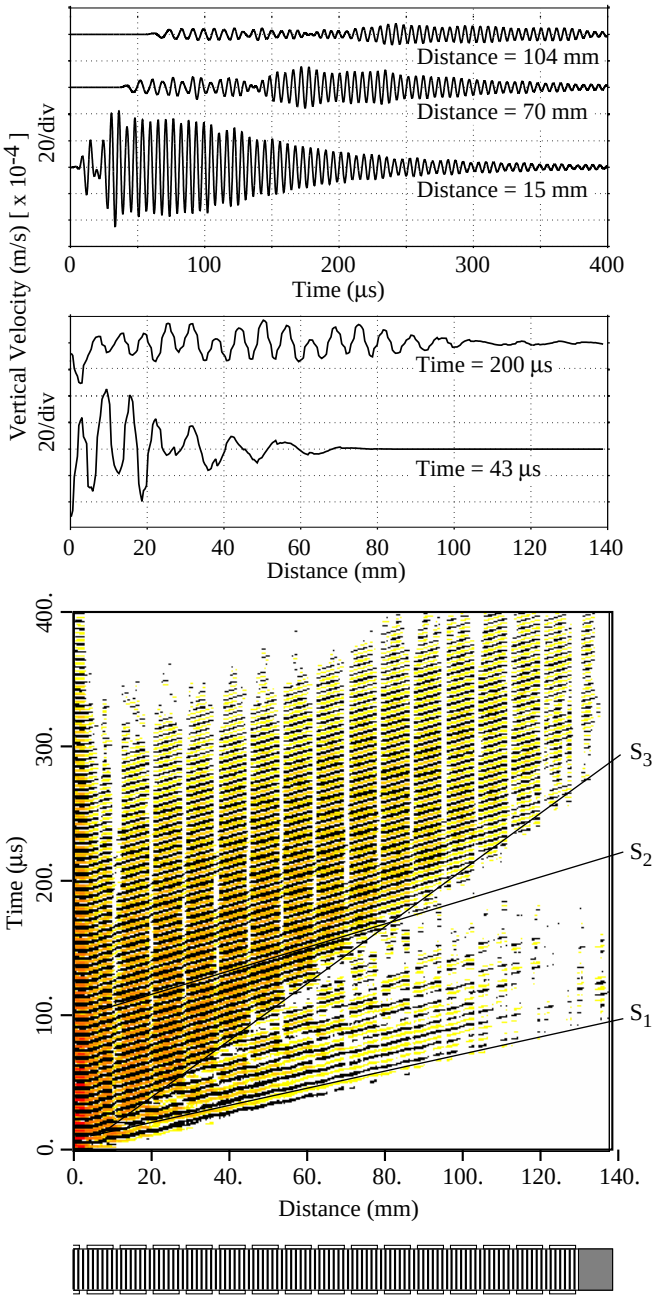

Figure 4. Dispersion analysis of the block in air from plot of normal velocity on the block surface versus time for each pillar position.

wavelength. An interesting observation is the left propagating group reflecting off the left end at ≈200 μs and continuing to the right as a coherent group to the top of the plot. This is Bragg scattering from the periodic pillars. It produces the low amplitude, long period oscillation seen in the velocity time-histories at the top of Figure 5.

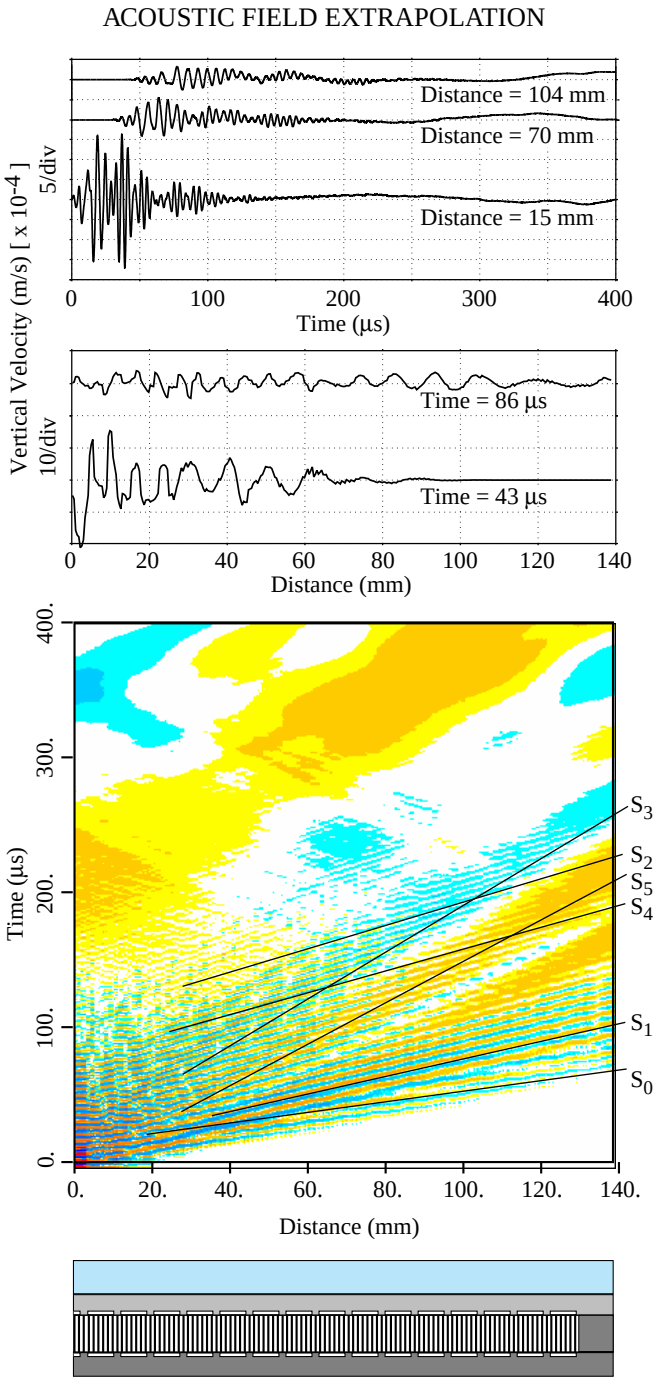

Figure 5. Dispersion analysis of the transducer in air from plot of normal velocity on the block surface versus time for each pillar position.

A comprehensive modeling capability must evaluate and manipulate accoustic fields over the homogeneous region in front of the transducer. However, computer memory limits the coverage, severely so in 3D. In addition, dispersion caused by propagating many wave lengths (i.e., hundreds) through a numerical grid distorts pulses unless the algorithm is specially optimized, at the expense of structural model performance. The recourse is, of course, to use some semi-analytical field extrapolation scheme in the water. The classical approach is the Kirchhoff integral on a surface surrounding all sources in the homogeneous, scalar (acoustic) medium. This involves integration of the source distribution and Greens function over a surface and over time for each output point. We have incorporated a time-domain Kirchhoff extrapolation algorithm in PZFlex, which will be described elsewhere.

Here we consider an attractive alternative, Fourier optics [25], which is simply a linear systems reformulation of Kirchhoff diffraction theory. In the case of projected fields it consists of a sequence of time- and space-Fourier transforms on pressure-time records over a plane (line) in front of the transducer, called the *object* plane. First, records are time-Fourier transformed into frequency spectra. Second, at each frequency the spatial distribution is space-Fourier transformed into angular spectra. This is the critical decomposition into evanescent and propagating plane waves at each frequency. Third, amplitude and phase of the plane waves are modified to account for propagation to the *image* plane through free space, apertures, and/or lenses. Fourth, the modified angular spectrum at each temporal frequency is inverse transformed

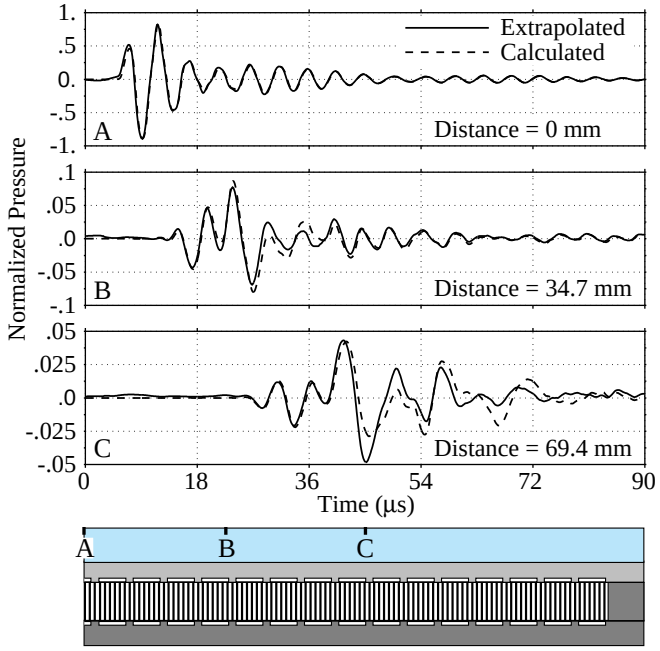

Figure 6. Validation of Fourier extrapolation of pressure on the wet side of the matching layer to points near the boundary of a shallow water layer.

giving temporal spectra on the image plane. And fifth, the temporal spectra are inverse transformed, yielding pressure-time records on the entire image plane. In practice this sequence of Fourier transforms is performed by the FFT algorithm on uniformly sampled space-time data.

In a sister code, EMFlex, we use Fourier optics to image light transmitted and diffracted by photomasks in submicron IC lithography [26]. A subset of these routines is applied to the transducer problem. Our validation example consists of the UDI transducer model with 8 mm of water beyond the matching layer, drawn in Figure 6. The left electrode is driven impulsively. Pressure just outside the matching layer over the model is extrapolated to a plane 2 mm below the top of the finite element acoustic domain. Extrapolated and finite element calculated pressures are compared there at three points. This is a typical example of how extrapolation is used, i.e., making the water very shallow in order to save elements for structural parts of the model. In this case the radiation boundary conditions are actively removing waves (and reflecting some unavoidable noise) for 88 μs during the extrapolation. The error observed in the extrapolation is the same magnitude at the three points and is caused by the background noise in the grid. It can be seen as a weak precursor before the real signal at points B and C.

NUMERICAL EXPERIMENTS

Besides its use in design, discrete numerical modeling is a useful experimental tool. For example, the designer can postulate interesting composite block or transducer configurations, test them on the computer (within the limits of memory and speed), and quickly focus design and experimental efforts on the most promising approaches. Numerical experiments are done here to look at effects of pillar shape and distribution. This is motivated by the geometrical freedom offered by injection molding, in contrast to the dice-and-fill method.

We consider the 500 kHz preliminary design sketched in Fig. 2 and look at the effect of pillar distribution on cross-talk. Every other pillar row, in azimuth say, of the 500 kHz layout is staggered 1/2 pitch (0.5 mm) and cross-talk to the first and second neighbor of the driven electrode is compared to that in the regular (Cartesian) distribution. The 3D model is 1/2 pitch in elevation for the regular spacing and 1 pitch for the staggered. It includes 1/2 of the driven electrode and two neighbors on one side. Cross-talk voltage is Fourier transformed and the spectra are normalized by the driving spectrum. Results are shown in Figure 7.

We also look at what effects pillar taper has on radiated sound. Initial models are 2D since all behaviors should be exhibited qualitatively. Three shapes are considered, each with the same volume fraction, namely, straight pillars, pillars tapered in one direction, and pillars tapered in both directions. Shapes are shown on the top of Figure 8. The bare plate is fully electroded and driven impulsively in water, without matching layer or backing. The pressure is measured 4.5 mm above and below the plate for each taper case, Fourier transformed, and cross-plotted in Figure 8.

SUMMARY AND CONCLUSIONS

Time-domain finite element modeling and is applied to 1-3 composites for underwater imaging arrays. The code used, PZFlex, often permits two orders of magnitude larger models or faster solutions than the implicit codes reported in the literature for transducer analyses. It is currently used by a number of commercial ultrasound companies. The composites modeled include a 150 kHz block built by UDI-Wimpol, Ltd. for an electronically scanned imaging sonar and a preliminary 500 kHz design for an ONR program. These studies set baselines for an active design collaboration with the Ultrasonics Research Group at the University of Strathclyde.

In preparation for code validation against more complete UDI experiments, we compare to measured voltage cross-talk for the block in air. Models are severely limited by incomplete material properties.

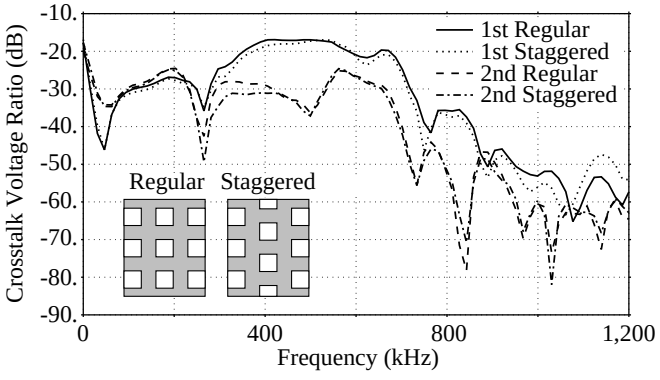

Figure 7. Cross-talk to the 1st and 2nd electrodes versus frequency for regular and staggered pillars in the 500 kHz composite design.

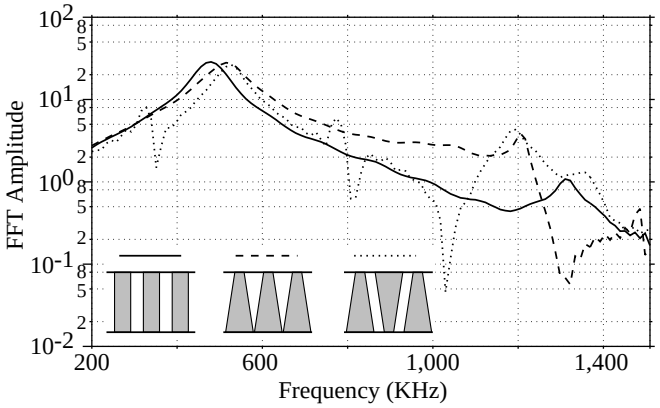

Figure 8. Pressure spectrum 4.5 mm in front of the three taper cases.

Nonetheless, correlation is reasonable in this case and serves as a qualified validation of the model until more complete material data are available. Note that from the dispersion analysis it is clear that arrival time errors in calculated cross-talk are caused by too high a shear velocity assumed in the polymer fill (1800 m/s versus 1500 m/s). This implies that the polymer's Poisson ratio should be increased from .4 to .45.

A 2D model is used to investigate dispersion behavior of the UDI composite—both the bare block in air and the potted block with matching layer and backing in water. This is done by plotting vertical velocity across the block's surface for an impulsive voltage applied at one electrode. Pictures delineate the various plate waves nicely, including coherent Bragg reflections and associated long period waves. Mode shapes and velocity polarization can also be examined for classifying phases.

Time-domain dispersion analysis is useful because it identifies cross-talk signals and suggests ways of reducing cross-talk in multi-electroded designs. For the composite in air, the first signal is from the horizontally propagating shear wave (S1) and subsequent lower amplitude ringing is from the plate wave group (S2). However, in air the plate wave group amplitude is higher than the shear wave, so why is its resulting cross-talk lower? This depends on the number of wavelengths under the electrode (width L). A simple calculation shows that cross-talk is proportional to $\lambda\sqrt{1-\cos(2\pi L/\lambda)}$. Therefore, signal is reduced in part because S2's wave length is about half of S1's. Furthermore, there is signal extinction for an integer number of wave lengths under the electrode ($L/\lambda = N$). If the Lamb-type wave length nearly satisfies this condition then additional cancellation will occur. Mode shape of each phase may also contribute to differences in cross-talk.

We demonstrate a Fourier optics (acoustics) algorithm that analytically models sound propagation in water outside the finite element grid. It transforms fields evaluated on an object plane to an image plane of the same size at any distance. The method is validated against a finite element calculation of the UDI 2D model in water and works as predicted. By imaging with and without evanescent wave truncation we find that evanescent waves are negligible beyond $\lambda_0/2$ from the matching layer. Fourier processing is fast compared to the time-domain Kirchhoff integral method but the amount of data can be prohibitive. Spectral truncation in angle and frequency should reduce memory requirements without degrading image quality. This Fourier approach will accommodate apertures, acoustic lenses, and simple reflectors in the analytical model.

Numerical experiments on pillar distribution and taper are done on a 2D, periodic model of the 500 kHz composite (uniformly electroded). The pillar distribution experiment did not indicate any dramatic effect near the design frequency. Projected pressure for the straight pillar and two forms of tapered pillar, all with the same PZT volume fraction, are compared. Taper tends to complicate the modal picture by lowering overtone frequency and increasing overtone amplitude. Uniform taper in one direction appears to produce higher peak pressures on the side of the composite plate with narrowing pillars.

These examples show that 1-3 composite transducer design issues can be addressed effectively with explicit time-domain finite element simulations. Most of the examples would have been impractical using implicit codes, either because of limited problem size or excessive run time. Despite our success here, *global* 3D models will remain impractical on workstations and PCs for the foreseeable future, but massively parallel supercomputers are a viable option. In the meantime, we expect that 2D simulations with averaged properties in the third dimension will be an effective intermediate solution in many transducer layouts.

ACKNOWLEDGMENTS

This work was supported under ONR Contract N00014-94-C-0047 and NSF SBIR Grant DMI-9313666 (G.L.W., D.K.V., and J.M., Jr.). We are pleased to acknowledge our benevolent ONR monitor, Dr. Wallace A. Smith.

REFERENCES

[1] R.E. Newnham, D.P. Skinner, and L.E. Cross, "Connectivity and piezoelectric-pyroelectric composites," *Materials Res. Bull.*, **17**, 525, 1978.

[2] W.A. Smith, "The role of piezocomposites in ultrasonic transducers," *Proc. IEEE Ultrason. Symp.*, 755-766, 1989.

[3] L.J. Bowen, R.L. Gentilman, H.T. Pham, D.F. Fiore, and K.W. French, "Injection molded fine-scale piezoelectric composite transducers," *Proc. IEEE Ultrason. Symp.*, **1**, 499-503, 1993.

[4] K. Lubitz, A. Wolff, and G. Preu, "Microstructuring technology," *Proc. IEEE Ultrason. Symp.*, **1**, 515-524, 1993.

[5] R. Krimholtz, D.A. Leedom, and G.L. Matthaei, "New equivalent circuits for elementary piezoelectric transducers," *Electron. Lett.*, **6**, No.13, 398-399, 1970.

[6] W.A. Smith and B.A. Auld, "Modeling 1-3 composite piezoelectrics: thickness-mode oscillations," *IEEE Trans. Ultrason. Ferroelec. Freq. Contr.*, **38**, 40-47, 1991.

[7] B.A. Auld, Acoustic Fields and Waves in Solids, Vol. 1 & 2, 2nd edition, Krieger, 1990.

[8] B.A. Auld and Y. Wang, "Acoustic wave vibrations in periodic composite plates," *Proc. IEEE Ultrason. Symp.*, 528, 1984.

[9] D.D.N. Hall, J. Bennett, and G. Hayward, "The design and evaluation of ultrasonic arrays using 1-3 connectivity composites," *SPIE Proc.*, Vol. 1733, 216-227, 1992.

[10] G.L. Wojcik, D.K. Vaughan, N. Abboud, and J. Mould, Jr., "Electromechanical modeling using explicit time-domain finite elements," *Proc. IEEE Ultrason. Symp.*, **2**, 1107-1112, 1993.

[11] G.L. Wojcik, D.K. Vaughan, and N. Abboud, "Electromechanical finite element models for ultrasound transducer analysis and design," NSF SBIR Phase I Report, ISI 9161050, 1993.

[12] H. Allik and T.J.R. Hughes, "Finite element method for piezoelectric vibration," *Int. Numer. Methods Engng.*, **2**, 151-157, 1970.

[13] H. Allik, K.M. Webman, and J.T. Hunt, "Vibrational response of sonar transducers using piezoelectric finite elements," *J. Acoust. Soc. Am.*, **56,** 1782-1792, 1974.

[14] Y. Kagawa and T. Yamabuchi, "Finite element simulation of two-dimensional electromechanical resonators," *IEEE Trans. Sonics Ultrason.*, **SU-21**, 1974.

[15] D. Boucher, M. Langier, and C. Maerfeld, "Computation of the vibrational modes for piezoelectric array transducers using a mixed finite element-perturbation method," *IEEE Trans. Sonics Ultrason.*, **SU-28**, 318-330, 1981.

[16] M. Naillon, R. Coursant, and F. Besnier, "Analysis of piezoelectric structures by a finite element method," *Acta Electronica*, **25**, 341-362, 1983.

[17] R. Lerch, "Finite element analysis of piezoelectric transducers," *Proc. IEEE Ultrasonic Symp.*, **2**, 643-654, 1988.

[18] G. Hayward and J. Hossack, "Computer models for the analysis and design of 1-3 composite transducers," *Ultrason. Int. 89 Conf. Proc.*, **2**, 531-536, 1989.

[19] P.C. Kohnke, ANSYS® Engineering Analysis System Theoretical Manual, Swanson Analysis Systems, Inc., P.O. Box 65, Houston, Pennsylvania 15342.

[20] R. Courant, K.O. Friedrichs, and H. Lewy, "Über die partiellen differenzengleichungen der mathematischen physik," *Math. Ann.*, **100**, 32, 1928.

[21] J. von Neumann and R.D. Richtmyer, "A method for the numerical calculation of hydrodynamical shocks," *J. Appl Phys.*, **21**, 232, 1950.

[22] T.L. Szabo, "Time domain wave equations for lossy media obeying a frequency power law," *J. Acoust. Soc. Am.*, **96** (1), 491-500, 1994.

[23] C. Desilets, Personal communication, Ultrasound Solutions, Inc., Edmonds, WA, U.S.A.

[24] G. Hayward and J. Bennett, Personal communication, Ultrasonics Research Group, University of Strathclyde, Glasgow, Scotland.

[25] J.W. Goodman, Introduction to Fourier Optics, McGraw-Hill Book Co., San Francisco, 1968.

[26] G. Wojcik, J. Mould, Jr., R. Ferguson, R. Martino, K.K. Low, "Some image modeling issues for I-line, 5x phase shifting masks," *SPIE Proc.*, Vol. 2197: Optical/Laser Microlithography VII, 1994.